© 2021. Published by The Company of Biologists Ltd | Journal of Cell Science (2021) 134, jcs253807. doi:10.1242/jcs.253807

RESEARCH ARTICLE

Regulation of cell quiescence–proliferation balance by Ca^{2+}–CaMKK–Akt signaling

Yi Xin, Jian Guan, Yingxiang Li and Cunming Duan*

ABSTRACT

Compared with our extensive understanding of the cell cycle, we have limited knowledge of how the cell quiescence–proliferation decision is regulated. Using a zebrafish epithelial model, we report a novel signaling mechanism governing the cell quiescence–proliferation decision. Zebrafish Ca^{2+}-transporting epithelial cells, or ionocytes, maintain high cytoplasmic Ca^{2+} concentration ($[Ca^{2+}]_c$) due to the expression of Trpv6. Genetic deletion or pharmacological inhibition of Trpv6, or reduction of external Ca^{2+} concentration, lowered the $[Ca^{2+}]_c$ and reactivated these cells. The ionocyte reactivation was attenuated by chelating intracellular Ca^{2+} and inhibiting calmodulin (CaM), suggesting involvement of a Ca^{2+} and CaM-dependent mechanism. Long-term imaging studies showed that after an initial decrease, $[Ca^{2+}]_c$ gradually returned to the basal levels. There was a concomitant decease in endoplasmic reticulum (ER) Ca^{2+} levels. Lowering the ER Ca^{2+} store content or inhibiting ryanodine receptors impaired ionocyte reactivation. Further analyses suggest that CaM-dependent protein kinase kinase (CaMKK) is a key molecular link between Ca^{2+} and Akt signaling. Genetic deletion or inhibition of CaMKK abolished cell reactivation, which could be rescued by expression of a constitutively active Akt. These results suggest that the quiescence–proliferation decision in zebrafish ionocytes is regulated by Trpv6-mediated Ca^{2+} and CaMKK–Akt signaling.

KEY WORDS: Trpv6, Intracellular Ca^{2+}, ER Ca^{2+}, Calcium, Calmodulin, Cell cycle, Ionocyte, Zebrafish

INTRODUCTION

Cellular quiescence is a non-proliferative cellular state found in many cell types. Cellular quiescence protects long-lived cells by reducing DNA replication, mRNA translation, gene transcription and metabolic activity, as these activities are accompanied by molecular damage (Cheung and Rando, 2013; Fiore et al., 2018). Maintaining a pool of quiescent stem and precursor cells that can be rapidly reactivated to expand a cell population upon stimulation or injury is critical for tissue homeostasis and repair (Cheung and Rando, 2013). This is of particular importance for tissues with high turnover rates, such as epithelia. Epithelial tissues serve as a barrier against external environments and play critical roles in nutrient absorption, gas exchange, ion exchange and protection (Guillot and Lecuit, 2013; Tai et al., 2019). As such, they are frequently exposed to external chemical insults, injury and/or pathogen exposures (Biteau et al., 2011). Although it is well appreciated that regulation of the quiescence–proliferation balance is critical for epithelial tissue homeostasis, regeneration and wound healing, the underlying molecular mechanisms are still not well defined.

To unravel molecular mechanisms governing the quiescence–proliferation decision, we have developed a zebrafish model in which a population of quiescent epithelial cells, known as ionocytes or Na^+-K^+-ATPase-rich (NaR) cells, can be induced to re-enter the cell cycle in response to experimental manipulations (Dai et al., 2014; Liu et al., 2017, 2020; Xin et al., 2019). NaR cells take up Ca^{2+} from the surrounding aquatic habitats to maintain body Ca^{2+} homeostasis (Yan and Hwang, 2019). They are functionally and molecularly similar to human renal and colon epithelial cells. In the adult stage, NaR cells are located in the intestine and kidney, as well as in the gills – a major osmoregulation organ in adult fish (Hwang, 2009). In the embryonic and larval stages, however, these cells are located on the epidermis of the yolk sac (Hwang, 2009), making them easily accessible for experimental manipulation and observation. Previous studies have shown that when zebrafish are kept in embryo medium containing physiological concentrations of Ca^{2+} (~0.2 mM Ca^{2+}), NaR cells are maintained in the quiescent state, which is characterized by a low cell division rate and undetectable Akt–Tor signaling activity. When transferred to low Ca^{2+} concentration embryo medium (containing 0.001 mM Ca^{2+}; referred to hereafter as low $[Ca^{2+}]$ stress treatment), these cells are reactivated to re-enter the cell cycle and undergo robust division. This action has been attributed to Igf1 receptor-mediated phosphoinositide 3-kinase (PI3K)–Akt–Tor signaling (Dai et al., 2014; Liu et al., 2017). This is similar to the reported roles of PI3K–Akt–mTOR signaling in reactivating mammalian and *Drosophila* adult stem cells (Chell and Brand, 2010; Chen et al., 2008, 2009; Ziegler et al., 2019, 2015), suggesting that an evolutionarily conserved mechanism is at work.

A hallmark of NaR cells is expression of the gene encoding transient receptor potential cation channel subfamily V member 6 (Trpv6), which is a constitutively open Ca^{2+} channel that functions as the first and rate-limiting step in the transcellular Ca^{2+} transport pathway (Dai et al., 2014; Pan et al., 2005; Xin et al., 2019). We have recently shown that Trpv6-mediated Ca^{2+} influx maintains a high level of cytoplasmic Ca^{2+} ($[Ca^{2+}]_c$) in these cells and that the high $[Ca^{2+}]_c$ suppresses Akt–Tor signaling via the protein phosphatase PP2A (Xin et al., 2019). This is critical in maintaining the quiescent state, because genetic deletion of *trpv6* or pharmacological inhibition of Trpv6 lowers the $[Ca^{2+}]_c$ and increases Akt–Tor signaling, which in turn leads to quiescence exit and cell cycle re-entry (Xin et al., 2019). Importantly, this mechanism is conserved in human colon epithelial carcinoma cells (Xin et al., 2019). The molecular links between the $[Ca^{2+}]_c$ and Akt activation, and subsequent NaR cell reactivation, however, remain unclear.

In this study, we investigated the role of intracellular Ca^{2+} signaling in NaR cell reactivation. We show that reducing Trpv6-

Department of Molecular, Cellular and Developmental Biology, University of Michigan, Ann Arbor, MI 48109, USA.

*Author for correspondence (cduan@umich.edu)

Y.X., 0000-0002-4443-1342; C.D., 0000-0001-6794-2762

Handling Editor: John Heath
Received 1 September 2020; Accepted 15 September 2021

mediated Ca^{2+} influx into NaR cells lowers the $[Ca^{2+}]_c$ initially, but the $[Ca^{2+}]_c$ gradually returns to basal levels, possibly due to increased Ca^{2+} efflux from the endoplasmic reticulum (ER). Ca^{2+} concentration changes activate the conserved calmodulin (CaM)-dependent protein kinase kinase (CaMKK), and CaMKK acts via Akt to promote NaR cell reactivation.

RESULTS

Lowering intracellular Ca^{2+} concentration increases NaR cell proliferation

We have previously reported that low $[Ca^{2+}]$ stress treatment or the deletion or inhibition of Trpv6 causes pre-existing NaR cells to re-enter the cell cycle and proliferate, resulting in elevated NaR cell numbers in the zebrafish larval yolk sac region (Dai et al., 2014; Liu et al., 2017; Xin et al., 2019). In this study, we used two recently developed reporter fish lines, *Tg(igfbp5a:GFP)* and *Tg(igfbp5a:GCaMP7a)* (Liu et al., 2017; Xin et al., 2019), which express GFP and GCaMP7a (a genetically encoded Ca^{2+} reporter) in NaR cells, respectively, to further investigate the relationship between Trpv6, $[Ca^{2+}]_c$ and NaR cell reactivation. As previously reported, *trpv6*$^{-/-}$*; Tg(igfbp5a:GFP)* fish had elevated rates of NaR cell proliferation compared to their wild-type siblings (Fig. 1A,B). Likewise, low $[Ca^{2+}]$ stress treatment increased NaR cell proliferation (Fig. 1C). In both *trpv6*$^{-/-}$ fish and low $[Ca^{2+}]$ stress-treated fish, the $[Ca^{2+}]_c$ in NaR cells was significantly lower compared to that in the controls (Xin et al., 2019) (Fig. 1F). Next, Trpv6-mediated Ca^{2+} influx was inhibited using either lanthanum chloride or sodium chloride. Lanthanum chloride is a Trpv6 inhibitor, although it can also affect other channels and can lead to a gradual depletion of ER Ca^{2+} stores (Kovacs et al., 2011). Although Trpv6 proteins are well-known as Ca^{2+}-selective channels, mammalian TRPV6 has also been shown to conduct Na^+, albeit with 100-fold lower affinity compared to Ca^{2+} (Voets et al., 2004). Therefore, when added at greater than 100-fold concentration, Na^+ reduces TRPV6-mediated Ca^{2+} influx by competition (Voets et al., 2004). Both lanthanum chloride and sodium chloride treatments reduced the $[Ca^{2+}]_c$ and increased NaR cell proliferation (Fig. 1D–F). In comparison, N-methyl-D-glucamine chloride [(NMDG)Cl] of the same concentration had no such effect, ruling out the possibility that this effect was caused by changes in osmolarity or Cl^- concentration (Fig. 1E,F). Akt signaling is essential for NaR cell reactivation, and Trpv6 knockout or inhibition increases Akt signaling in NaR cells (Dai et al., 2014; Liu et al., 2017; Xin et al., 2019). Consistent with this notion, immunostaining results showed that lanthanum chloride and sodium chloride treatments increased the number of phosphorylated Akt-positive NaR cells, whereas (NMDG)Cl had no such effect (Fig. S1). Taken together, these results suggest that lowering $[Ca^{2+}]_c$ in NaR cells is associated with increased Akt signaling and elevated cell proliferation.

NaR cell reactivation requires ER Ca^{2+}

To further explore the role of Ca^{2+} in NaR cell reactivation, *Tg(igfbp5a:GFP)* fish were treated with BAPTA-AM, an intracellular Ca^{2+} chelator. Interestingly, the low $[Ca^{2+}]$ stress treatment-induced NaR cell reactivation was significantly reduced by BAPTA-AM treatment (Fig. 2A). This effect was not due to BAPTA-AM toxicity, because BAPTA-AM treatment did not affect embryo viability (Fig. S2). When *Tg(igfbp5a:GFP)* fish were treated with W-7 hydrochloride and calmidazolium chloride, two CaM antagonists, the low $[Ca^{2+}]$ stress treatment-induced NaR cell reactivation was impaired (Fig. 2B). These findings suggest that intracellular Ca^{2+} and CaM activity are important for NaR cell reactivation. We next performed long-term *in vivo* Ca^{2+}-imaging experiments. Although the low $[Ca^{2+}]$ stress treatment significantly decreased NaR cell $[Ca^{2+}]_c$ levels in the first 2 h, the $[Ca^{2+}]_c$ gradually returned to the control levels after 18 h (Fig. 2C,D), which may explain the observed inhibitory effects of BAPTA-AM, W-7 hydrochloride and calmidazolium chloride.

The abovementioned results indicate that an intracellular source of Ca^{2+} may be involved. The ER is the major intracellular Ca^{2+} store (Clapham, 2007; Luchsinger et al., 2019). To investigate whether ER Ca^{2+} replenishes Ca^{2+} in the cytosol, we measured the ER Ca^{2+} concentration, $[Ca^{2+}]_{ER}$, using a genetically-encoded ER Ca^{2+} indicator, ER-LAR-GECO-1 (Wu et al., 2014). The $[Ca^{2+}]_{ER}$ decreased after 18 h (Fig. 2E,F). The possible involvement of ER Ca^{2+} was examined using thapsigargin and cyclopiazonic acid, two distinct inhibitors of the sarco/endoplasmic reticulum Ca^{2+}-ATPase (SERCA, also known as Atp2a1 in zebrafish). Thapsigargin treatment significantly inhibited low $[Ca^{2+}]$ stress treatment-induced NaR cell reactivation (Fig. 3A,B). Cyclopiazonic acid had a similar effect (Fig. 3A,B). Co-treatment with Z-VAD-fmk, an anti-apoptotic agent validated in zebrafish embryos (Kamei et al., 2018), had no effect in NaR cells in the presence or absence of thapsigargin (Fig. 3C), indicating that apoptosis is not a major factor.

Store-operated Ca^{2+} entry (SOCE) can be activated by chelating intracellular Ca^{2+}, depleting ER Ca^{2+} or treating cells with SERCA inhibitors, including thapsigargin. To explore the possible involvement of SOCE, we used CRISPR/Cas9 to knockdown Stim1a, a key player in SOCE (Prakriya and Lewis, 2015). Stim1a knockdown did not affect NaR cell reactivation or basal NaR cell number (Fig. 3D; Fig. S3). ER Ca^{2+} efflux is mediated by ryanodine receptors (RyRs) and/or inositol (1,4,5)-trisphosphate receptors (IP3Rs) (Gonano and Jones, 2017; MacMillan, 2013). Treatment of zebrafish larvae with the RyR inhibitors ryanodine and dantrolene blocked NaR cell reactivation (Fig. 3E,F), whereas the IP3R inhibitor xestospongin C did not have such effect (Fig. S4). Collectively, these data suggest that ER Ca^{2+} efflux mediated by RyRs is involved in NaR cell reactivation.

ER Ca^{2+} efflux activates CaMKK–Akt signaling to promote cell reactivation

Activation of Akt signaling is essential for NaR cell cycle re-entry (Dai et al., 2014; Liu et al., 2017; Xin et al., 2019). Immunostaining results showed that BAPTA-AM, W-7 hydrochloride and calmidazolium chloride treatments all reduced phosphorylated Akt (phospho-Akt) levels (Fig. 4A–C). Thapsigargin treatment also reduced phospho-Akt levels in a dose-dependent manner (Fig. 4D), suggesting that Ca^{2+} may regulate NaR cell reactivation via Akt. If this is correct, then constitutive activation of Akt should reverse the inhibition by thapsigargin. This idea was tested by targeted expression of myrAkt, a constitutively active form of Akt (Kohn et al., 1996), in NaR cells using a Tol2 transposon BAC-mediated genetic mosaic assay (Liu et al., 2018). Whereas thapsigargin treatment significantly inhibited NaR cell reactivation in the control group, this effect was not observed in NaR cells expressing myrAkt (Fig. 4E).

In a previous chemical biology screen performed using *Tg(igfbp5a:GFP)* larvae (Xin et al., 2019), a number of compounds were found to block NaR cell reactivation. Among them was STO-609, a known CaMKK inhibitor. CaMKK has been reported to phosphorylate AKT1 at T308 in cultured human cells (Chen et al., 2002; Gocher et al., 2017; Ma et al., 2016; Schmitt et al., 2012; Wang et al., 2015; Yano et al., 1998). We therefore hypothesized that CaMKK may be the molecule linking Ca^{2+} to

Journal of Cell Science (2021) 134, jcs253807. doi:10.1242/jcs.253807

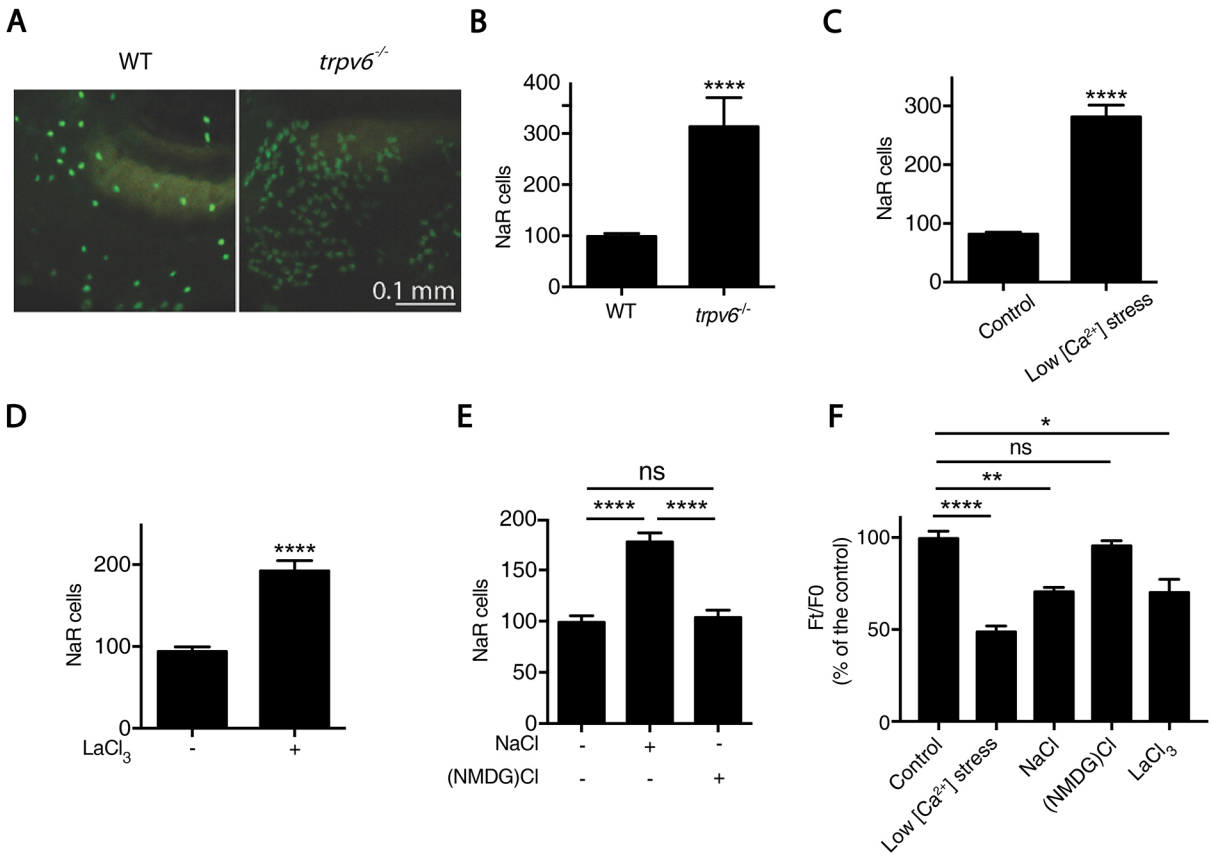

Fig. 1. Elevated NaR cell proliferation is associated with reduced cytoplasmic Ca^{2+} levels. (A,B) Progeny of *trpv6* $^{+/-}$; *Tg(igfbp5a:GFP)* intercrosses were raised in E3 embryo medium until 5 dpf. NaR cell number in each larva was quantified followed by individual genotyping. Representative images of wild-type (WT) and *trpv6*$^{-/-}$ larvae are shown in A, and quantified results are shown in B. WT, *n*=36; *trpv6*$^{-/-}$, *n*=14. For images, lateral views of the zebrafish yolk sac region are shown, with the dorsal side positioned to the top and the anterior to the left. (C) *Tg(igfbp5a:GFP)* fish raised in E3 embryo medium were transferred to normal [Ca^{2+}] (control) or low [Ca^{2+}] embryo media (low [Ca^{2+}] stress) at 3 dpf. NaR cell number in each larva was quantified at 5 dpf. Control, *n*=11; low [Ca^{2+}] stress, *n*=17. (D) *Tg(igfbp5a:GFP)* embryos raised in E3 embryo medium were transferred to normal [Ca^{2+}] embryo medium with or without 100 µM $LaCl_3$ at 3 dpf. Two days later, NaR cell number in each fish was quantified. *n*=12. (E) *Tg(igfbp5a:GFP)* embryos raised in E3 embryo medium were transferred to normal [Ca^{2+}] embryo medium containing 100 mM NaCl or 100 mM (NMDG)Cl at 3 dpf. Two days later, NaR cell number in each fish was quantified. *n*=8–13. (F) *Tg(igfbp5a:GCaMP7a)* embryos were injected with *BAC (igfbp5a:mCherry)* and raised to 3 dpf. They were transferred to normal [Ca^{2+}] embryo medium (control), low [Ca^{2+}] embryo medium (low [Ca^{2+}] stress) or normal [Ca^{2+}] embryo medium containing 100 mM NaCl, 100 mM (NMDG)Cl or 100 µM $LaCl_3$. Change in GCaMP7a signal intensity before and after treatment (F_t/F_0) was recorded, normalized to the mCherry signal intensity and expressed as a percentage of the control group value. *n*=20. Data in B–F are presented as mean±s.e.m. **P*<0.05; ***P*<0.01; *****P*<0.0001; ns, not significant (two-tailed unpaired t-test in B–D; one-way ANOVA followed by Tukey's multiple comparison test in E,F).

Akt signaling and, consequently, to NaR cell reactivation. Indeed, STO-609 treatment abolished NaR cell reactivation in *trpv6*$^{-/-}$ mutant fish (Fig. 5A). STO-609 also inhibited low [Ca^{2+}] stress- and NaCl treatment-induced NaR cell reactivation (Fig. 5B,C). The zebrafish genome has three CaMKK genes, *camkk1a*, *camkk1b* and *camkk2*. CRISPR/Cas9-mediated knockdown of these genes impaired low [Ca^{2+}] stress treatment-induced NaR cell reactivation (Fig. 5D,E; Fig. S5). If CaMKK indeed stimulates NaR cell reactivation by phosphorylating Akt, then STO-609 treatment should reduce Akt phosphorylation levels. Conversely, constitutive activation of Akt should reverse the effect of CaMKK inhibition. As shown in Fig. 6A and B, STO-609 treatment significantly reduced the number of T308 and S473 phospho-Akt-positive NaR cells. Expression of myrAkt increased NaR cell proliferation under normal Ca^{2+} concentration conditions, and this increase was not affected by STO-609 treatment (Fig. 6C). NaR cell reactivation induced by low [Ca^{2+}] stress treatment was significantly reduced by STO-609 treatment. In the myrAkt expression group, however, STO-609 treatment did not inhibit NaR cell reactivation (Fig. 6D).

DISCUSSION

Ca^{2+} is a ubiquitous intracellular signaling molecule involved in many aspects of cellular functions. Previous studies have implicated intracellular Ca^{2+} in the quiescence–proliferation decision in stem cells. Horsley et al. (2008) reported that high intracellular Ca^{2+} levels in mouse hair stem cells promote cell quiescence via calcineurin, a Ca^{2+}-regulated serine/threonine phosphatase, and its downstream effector nuclear factor of activated T cells (NFAT) (Horsley et al., 2008). In zebrafish, Ca^{2+} influx in response to GABA-A receptor activation regulates melanocyte stem cell quiescence via calcineurin (Allen et al., 2019). In a recent study, we have found that Trpv6-mediated Ca^{2+} influx maintains NaR cell quiescence via the action of another serine/threonine protein phosphatase, PP2A (Xin et al., 2019). These studies suggest that high cytoplasmic Ca^{2+} levels promote cell quiescence. On the other hand, Umemoto et al. (2018) reported that mouse hematopoietic stem cells (HSCs) undergo division because of increased intracellular Ca^{2+} level. Likewise, Luchsinger et al. (2019) reported that quiescent HSCs in the mouse bone marrow maintain low intracellular Ca^{2+} levels and that low Ca^{2+} treatment promotes

Journal of Cell Science (2021) 134, jcs253807. doi:10.1242/jcs.253807

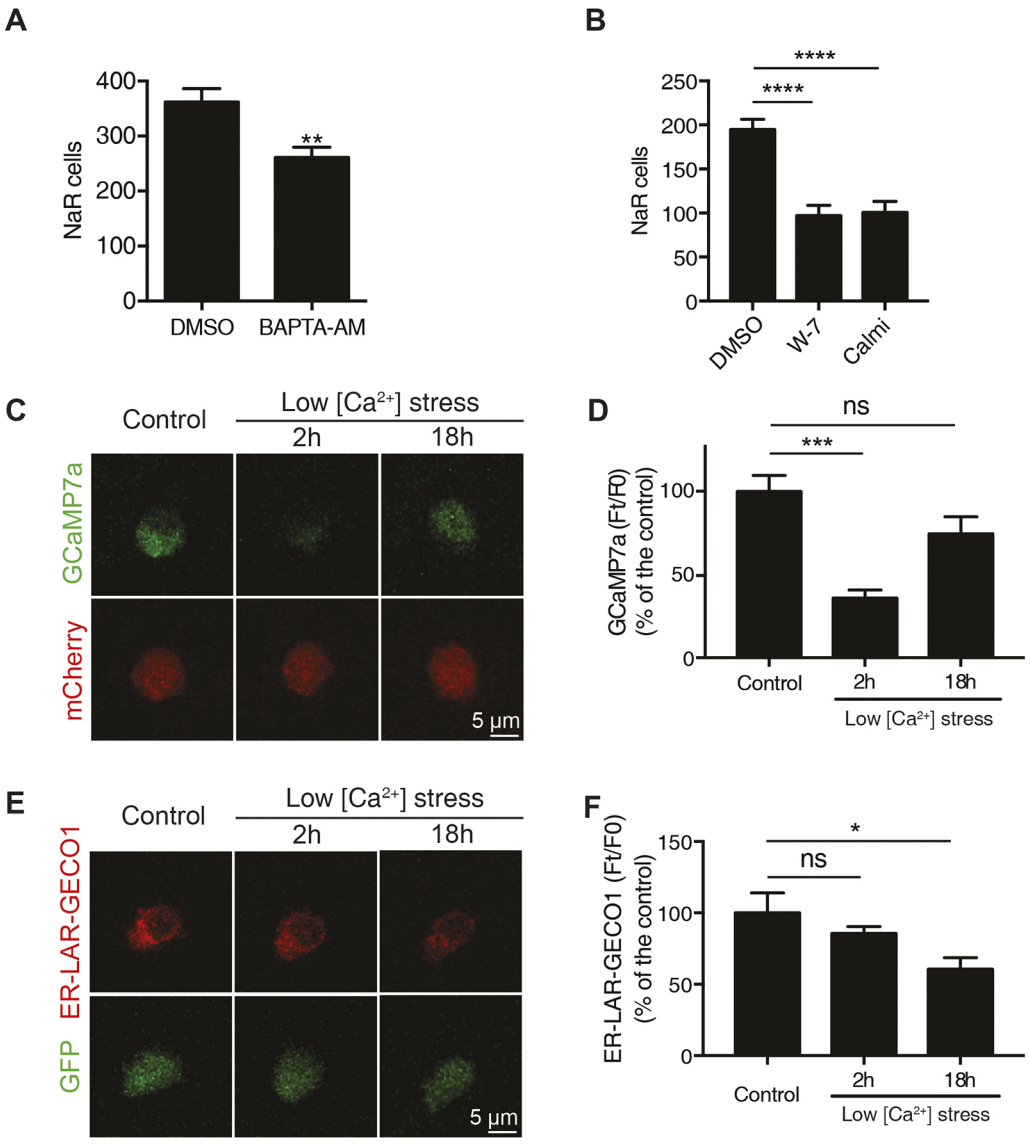

Fig. 2. Ca^{2+}/CaM activity is critical in NaR cell reactivation. (A) Effect of BAPTA-AM treatment. Wild-type larvae were transferred to low [Ca^{2+}] medium containing DMSO or 100 µM BAPTA-AM at 3 dpf. At 5 dpf, they were fixed. Because they were wild-type fish, the NaR cells were detected by *in situ* hybridization using a *trpv6* cRNA probe. NaR cell number in each fish was manually quantified. *n*=21–23. (B) *Tg(igfbp5a:GFP)* embryos were transferred to low [Ca^{2+}] embryo medium containing DMSO, W-7 hydrochloride (W-7, 50 µM) or calmidazolium chloride (Calmi, 1 µM) at 3 dpf. At 5 dpf, NaR cell number in each fish was quantified. *n*=21–23. (C,D) Changes in $[Ca^{2+}]_c$. *Tg(igfbp5a:GCaMP7a)* embryos were injected with *BAC (igfbp5a:mCherry)* at one-cell stage and raised until 3 dpf. They were imaged before transferring to the low [Ca^{2+}] embryo medium (control) and at the indicated times after transfer to the low [Ca^{2+}] stress conditions. GCaMP7a and mCherry signal intensity in the same NaR cell was measured, and the normalized change in GCaMP7a signal is expressed as percentage of the control group value. Representative images are shown in C, and quantified results are shown in D. *n*=6. (E,F) Changes in $[Ca^{2+}]_{ER}$. *Tg(igfbp5a:GFP)* embryos were injected with *BAC (igfbp5a:ER-LAR-GECO-1)* at one-cell stage. The injected embryos were raised until 3 dpf. They were imaged before transferring to the low [Ca^{2+}] embryo medium (control) and at the indicated times after transfer to the low [Ca^{2+}] stress conditions. The ER-LAR-EGCO1:GFP signal intensity ratio in the same NaR cell was measured and quantified as described in the Materials and Methods, and is expressed as a percentage of the control group value. Representative images are shown in E, and the quantified results are shown in F. *n*=8. Data in A,B,D and F are presented as mean±s.e.m. For images in C and E, single NaR cells are shown. **P*<0.05; ***P*<0.01; *****P*<0.0001; ns, not significant (two-tailed unpaired *t*-test in A; one-way ANOVA followed by Tukey's multiple comparison test in B,D,F).

quiescence when tested in cultured HSCs *in vitro*. This low Ca^{2+} concentration effect was linked to calpains, a family of Ca^{2+}-dependent cysteine proteases. Lower calpain activity under low $[Ca^{2+}]_c$ contributes to HSC maintenance via stabilization of Tet enzymes (Luchsinger et al., 2019). The reason(s) underlying these opposite effects of intracellular Ca^{2+} and CaM activity are not clear, but they are key to our understanding of the role of intracellular Ca^{2+} signaling in the regulation of quiescence–proliferation decisions. In this study, we provide evidence that the dynamics of $[Ca^{2+}]_c$ changes and the source of Ca^{2+} are critical. Furthermore, Ca^{2+} signal acts through CaMKK to increase Akt signaling and promote cell cycle re-entry.

Previous studies have shown that Trpv6 plays a key role in mediating external Ca^{2+} entering the cell and in maintaining high $[Ca^{2+}]_c$ in NaR cells (Xin et al., 2019). In addition to extracellular sources of Ca^{2+}, intracellular organelles such as the ER contain high concentrations of Ca^{2+} and function as internal Ca^{2+} stores (Bagur and Hajnoczky, 2017; Yang et al., 2019). Using zebrafish lines

Journal of Cell Science (2021) 134, jcs253807. doi:10.1242/jcs.253807

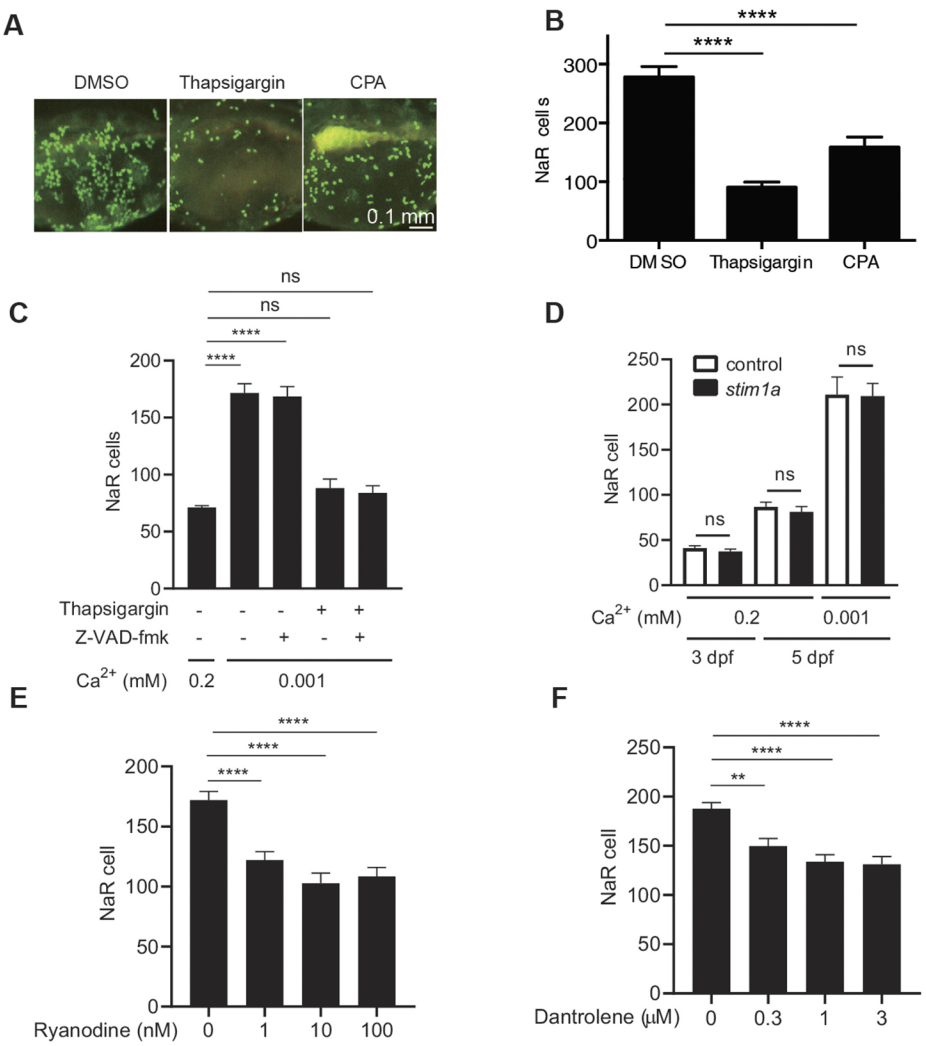

Fig. 3. ER Ca^{2+} signaling is involved in NaR cell reactivation. (A,B) Effects of thapsigargin and cyclopiazonic acid (CPA). *Tg(igfbp5a:GFP)* fish were transferred to low [Ca^{2+}] embryo media containing DMSO, 0.25 µM thapsigargin or 5 µM CPA at 3 dpf. Two days later, NaR cell number in each fish was quantified. Representative images are shown in A, and quantified results are shown in B. *n*=10–13. For images, lateral views of the zebrafish yolk sac region are shown, with the dorsal side positioned to the top and the anterior to the left. (C) Effect of thapsigargin and Z-VAD-fmk. *Tg(igfbp5a:GFP)* embryos were treated with DMSO, 0.25 µM thapsigargin and/or 50 µM Z-VAD-fmk in the indicated [Ca^{2+}] media from 3 dpf to 5 dpf. NaR cell number in each fish was quantified. *n*=12–15. (D) Effect of *stim1a* knockdown. *Tg(igfbp5a:GFP)* embryos were injected with a mixture of *stim1a*-targeting gRNAs and *cas9* mRNA (stim1) or gRNAs alone (control) at the one-cell stage. Injected embryos were raised in E3 embryo medium until 3 dpf and were then transferred to the indicated [Ca^{2+}] media. At 5 dpf, NaR cell number in each larva was quantified. *n*=7–25. (E,F) Effects of ryanodine (E) and dantrolene (F). *Tg(igfbp5a:GFP)* larvae were treated with DMSO, ryanodine or dantrolene at the indicated concentrations in low [Ca^{2+}] medium from 3 dpf to 5 dpf. NaR cells in each larva were quantified at 5 dpf. *n*=27–28 (E) or *n*=19–23 (F). Data in B–F are presented as mean±s.e.m. $^{**}P<0.01$; $^{****}P<0.0001$; ns, not significant (one-way ANOVA followed by Tukey's multiple comparison test in B,C,E,F; two-tailed unpaired *t*-test in D).

reporting $[Ca^{2+}]_c$ and $[Ca^{2+}]_{ER}$ levels, we provided data showing that the low [Ca^{2+}] stress treatment-induced $[Ca^{2+}]_c$ changes are more dynamic than previously thought. After an initial decrease, $[Ca^{2+}]_c$ gradually returned to the basal levels. This was accompanied by a concomitant decrease in ER Ca^{2+} levels. Furthermore, reducing ER Ca^{2+} contents by inhibiting ER Ca^{2+}-ATPase impaired NaR cell reactivation. Likewise, inhibition of RyRs inhibited NaR cell reactivation. In comparison, the IP3R inhibitor xestospongin C had no such effect. These results suggest that ER Ca^{2+} efflux via RyRs is critical. The mechanism of ER Ca^{2+} store regulation in NaR cell reactivation and how RyRs are activated during the low [Ca^{2+}] stress treatment, however, remain to be fully elucidated.

A key finding made in this study is that CaMKKs play a key role in linking Ca^{2+} signaling to NaR cell reactivation via Akt signaling (Fig. 6E). This conclusion is supported by the fact that treatment with a CaMKK inhibitor suppressed NaR cell reactivation. Likewise, CRISPR/Cas9-mediated knockdown of *camkk* genes abolished NaR cell reactivation. This conclusion is also supported by the findings that W-7 hydrochloride and calmidazolium chloride decreased NaR cell reactivation. Likewise, the intracellular chelating agent BAPTA-AM inhibited NaR cell reactivation. CaMKKs are monomers that are maintained in an inactive state by their autoinhibitory domain, which interacts with the catalytic domain to suppress kinase activity (Swulius and Waxham, 2008). Binding of Ca^{2+}/CaM relieves this inhibition by displacing the autoinhibitory domain and exposing the catalytic site. This leads to the activation of CaMKK and the subsequent phosphorylation of its downstream substrates (Tokumitsu and Soderling, 1996). Yano et al. (1998) reported that CaMKK directly phosphorylates AKT1 at T308 in cultured mammalian cells. This regulation has been observed in prostate epithelium-derived cancer cells and other cancer cells (Gocher et al., 2017; Schmitt et al., 2012; Wang et al., 2015). In zebrafish NaR cells, genetic deletion of CaMKK or inhibition of CaM and CaMKK significantly reduced the number of phospho-Akt-positive NaR cells. Using genetic mosaic assays, we showed that constitutive activation of Akt rescued NaR cell reactivation in the CaMKK-deficient state. These findings argue that CaMKK stimulates NaR cell reactivation via activation of Akt (Fig. 6E).

Although elevated CaMKK expression and activities have been implicated in the development and progression of liver, gastric, ovarian and prostate cancers (Berchtold and Villalobo, 2014; Gocher et al., 2017; Kahl and Means, 2003; Karacosta et al., 2012; Lin et al., 2015; Liu et al., 2016; Olianas et al., 2018; Shima et al., 2012; Subbannayya et al., 2015), the underlying mechanisms are still not well understood. The discovery made in this study has raised the question of whether Ca^{2+}–CaMKK–Akt signaling plays a general role in cell cycle regulation. Our results also raise the question as to how CaMKKs are activated under low [Ca^{2+}] stress. It

Journal of Cell Science (2021) 134, jcs253807. doi:10.1242/jcs.253807

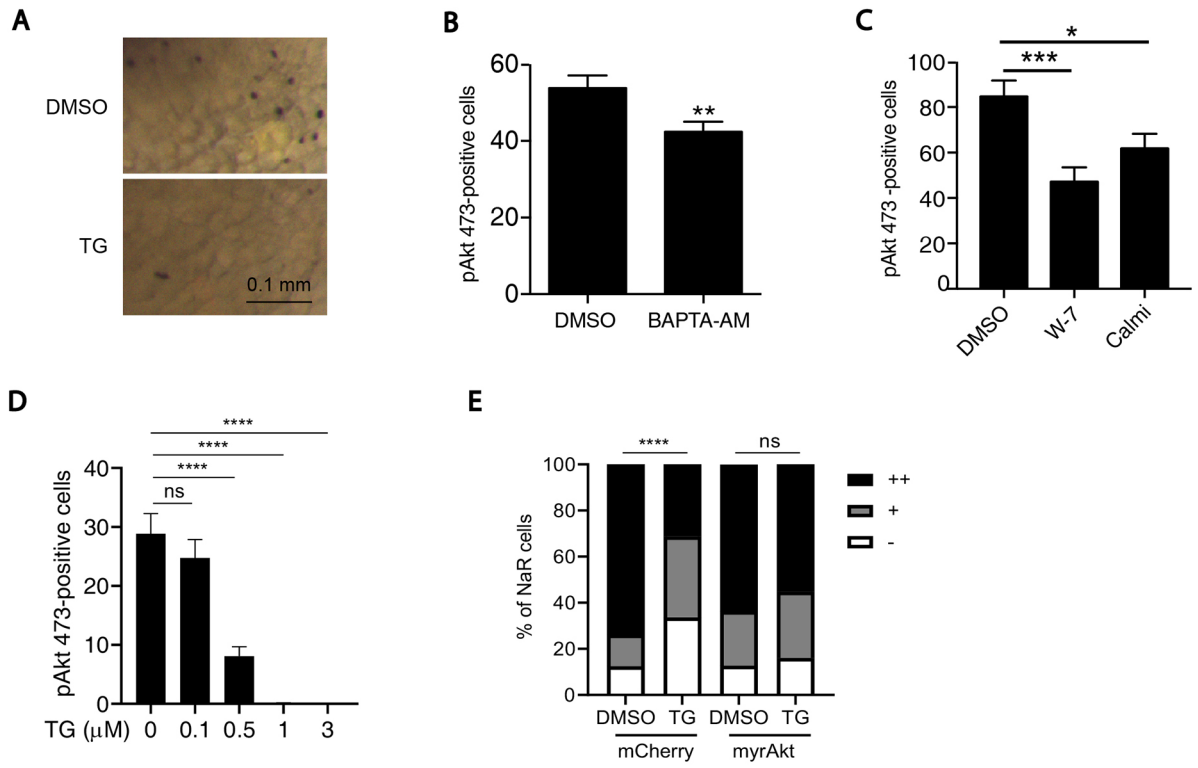

Fig. 4. ER Ca^{2+} efflux regulates NaR cell reactivation via Akt. (A) Representative images of phospho-Akt immunostaining (dark color) in thapsigargin (TG)-treated and control (DMSO) wild-type fish. Images show lateral views of the zebrafish yolk sac region, with the dorsal side positioned to the top and the anterior to the left. (B) Wild-type fish were transferred to low [Ca^{2+}] embryo media containing DMSO or 100 µM BAPTA-AM at 3 dpf. One day later, they were subjected to phospho-Akt (S473) immunostaining. The number of NaR cells positive for phospho-Akt (S473) in the yolk sac region was quantified. DMSO, *n*=13; BAPTA-AM, *n*=16. (C,D) Wild-type embryos were transferred at 3 dpf to low [Ca^{2+}] embryo media containing (C) DMSO, W-7 hydrochloride (W-7, 50 µM) or calmidazolium chloride (Calmi, 1 µM), or (D) thapsigargin at the indicated concentrations. One day later, they were immunostained and quantified as described in B. *n*=11–32. One-way ANOVA followed by Tukey's multiple comparison test. ns, no statistical difference. (E) Effect of myrAkt. One-cell-stage *Tg(igfbp5a:GFP)* embryos were injected with *BAC(igfbp5a:myr-Akt-mCherry)* or *BAC(igfbp5a:mCherry)* (mCherry control) and raised until 3 dpf. They were transferred to low [Ca^{2+}] embryo medium containing DMSO or thapsigargin (0.5 µM) at 3 dpf. At 5 dpf, NaR cells labeled by both GFP and mCherry were scored following a previously established scoring system (Liu et al., 2018). NaR cells that did not divide, divided once or divided twice are scored as –,+and++, respectively. *n*=8–12. Data in B–D are presented as mean±s.e.m. **P*<0.05; ***P*<0.01; ****P*<0.001; *****P*<0.0001; ns, not significant (two-tailed unpaired *t*-test in B; one-way ANOVA followed by Tukey's multiple comparison test in C,D; chi-square test in E).

has been reported that the release of ER Ca^{2+} via RyRs can result in a sharp increase in [Ca^{2+}] locally, creating Ca^{2+} microdomains without changing the global [Ca^{2+}]$_c$ (Bagur and Hajnoczky, 2017). Ca^{2+} microdomains regulate specific cellular processes in different regions of a cell, given that the actions of local Ca^{2+} signals may be restricted to effectors located within sub-micrometer distances from the Ca^{2+} source (Carafoli and Krebs, 2016). Future studies are needed to determine whether Ca^{2+} microdomains form in NaR cells and play a causational role in regulating cell quiescence–proliferation decisions. Humans have two CaMKK isoforms. In zebrafish, there are three *camkk* isoforms. In mammals, there are three AKT isoforms: AKT1, AKT2 and AKT3. In zebrafish, five Akt isoforms have been identified, including Akt1, Akt2, Akt2-like (Akt2l), Akt3a and Akt3b (Chen et al., 2017). Future studies are needed to clarify the relationships between these different CaMKK and Akt isoforms and determine the specific isoforms involved in the cell quiescence–proliferation decision.

Limitations of the study

NaR cells are epithelial cells specialized in transcellular transport of Ca^{2+} (Yan and Hwang, 2019). These cells maintain high [Ca^{2+}]$_c$ due to the expression of Trpv6. This conclusion is supported by published results showing that (1) Trpv6 is a constitutively open Ca^{2+} channel (Xin et al., 2019); (2) *trpv6* is highly and exclusively expressed in NaR cells (Dai et al., 2014; Liu et al., 2017; Pan et al., 2005); (3) genetic deletion, pharmacological blockade and competitive inhibition of Trpv6 reduced the [Ca^{2+}]$_c$ (Xin et al., 2019); (4) re-expression of Trpv6 or washing out the inhibitors restored the [Ca^{2+}]$_c$ (Xin et al., 2019); and (5) importantly, addition of ionomycin did not result in a major increase in the basal [Ca^{2+}]$_c$ (Xin et al., 2019), indicating that the endogenous [Ca^{2+}]$_c$ is indeed very high. The precise [Ca^{2+}]$_c$ in NaR cells, however, is unknown due to the lack of tools for measuring endogenous [Ca^{2+}]$_c$ in these cells *in vivo*. Future studies are needed to develop tools to reliably measure the precise [Ca^{2+}]$_c$ in NaR cells in zebrafish embryos and larvae.

In this study, [Ca^{2+}]$_{ER}$ was measured using a red fluorescent ER indicator, ER-LAR-GECO-1. ER-LAR-GECO-1 has been used to image ER- and mitochondrial-Ca^{2+} dynamics in cultured human cells (Wu et al., 2014). It was chosen in our study to monitor [Ca^{2+}]$_{ER}$ in GFP-labeled NaR cells. It should be pointed out that ER-LAR-GECO-1 has several limitations. ER-LAR-GECO-1 has a Ca^{2+} K_d value of 24 µM. Although the precise [Ca^{2+}]$_{ER}$ in NaR cells is unknown, [Ca^{2+}]$_{ER}$ can reach sub-millimolar ranges in most cell types (Clapham, 2007; Suzuki et al., 2014). Therefore, this sensor may have underestimated the basal [Ca^{2+}]$_{ER}$ signal. Another limitation is that ER-LAR-GECO-1 is not a ratiometric Ca^{2+} sensor. As such, both changes in the [Ca^{2+}]$_{ER}$ levels and changes in ER-LAR-GECO-1 protein levels can lead to variations in fluorescence

Journal of Cell Science (2021) 134, jcs253807. doi:10.1242/jcs.253807

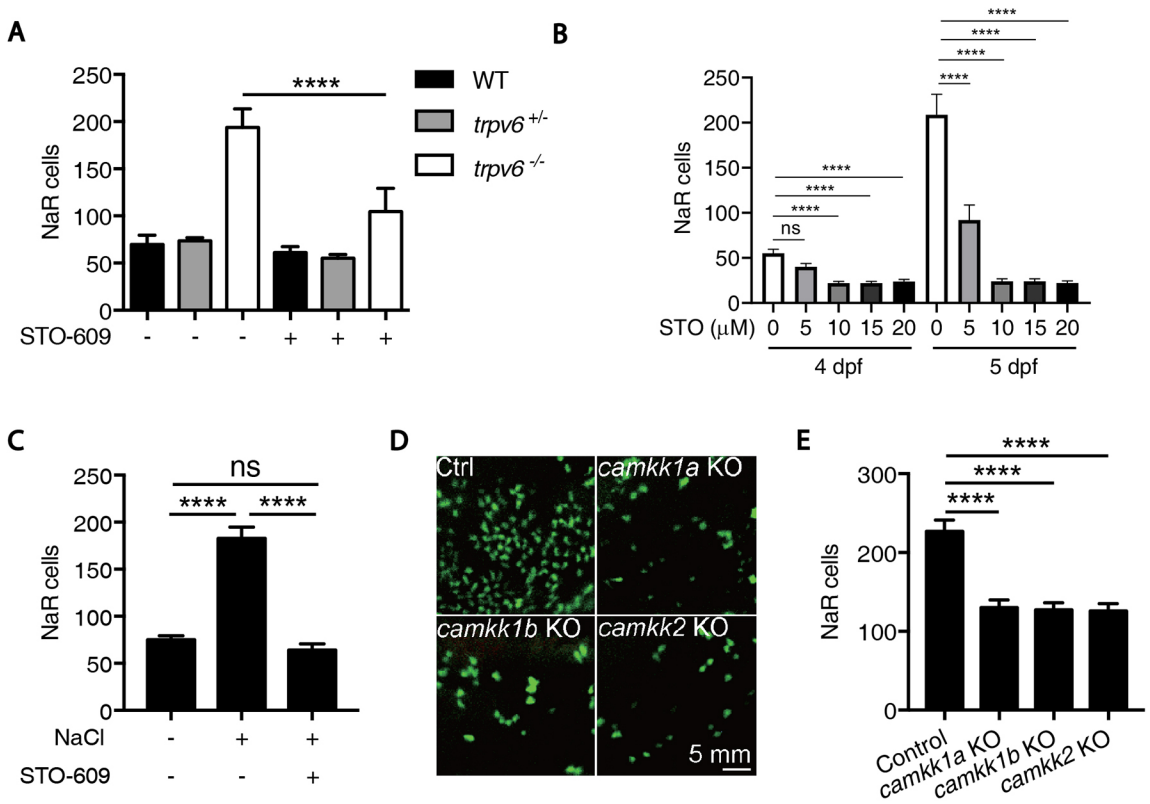

Fig. 5. CaMKK is required in NaR cell reactivation. (A) Progenies of *trpv6*$^{+/-}$; *Tg(igfbp5a:GFP)* intercrosses were transferred to normal [Ca^{2+}] embryo medium containing DMSO or 5 µM STO-609 at 3 dpf. At 5 dpf, NaR cell number in each larva was quantified, followed by individual genotyping (WT, wild-type larvae). *n*=12–41. (B) *Tg(igfbp5a:GFP)* larvae were transferred at 3 dpf to low [Ca^{2+}] embryo medium containing DMSO or STO-609 at the indicated concentrations. NaR cell number in each fish was quantified at 4 and 5 dpf. *n*=3–15. (C) *Tg(igfbp5a:GFP)* larvae were transferred to normal [Ca^{2+}] embryo medium containing 100 mM NaCl and/or 10 µM STO-609 at 3 dpf. At 5 dpf, NaR cell number in each fish was quantified. *n*=21–24. (D,E) Knockout (KO) of *camkk* genes. *Tg(igfbp5a:GFP)* fish were injected at one-cell stage with gRNA targeting the indicated *camkk* gene and *cas9* mRNAs, or with gRNAs alone (control, Ctrl). The injected embryos were raised and transferred to low [Ca^{2+}] embryo medium at 3 dpf. At 5 dpf, NaR cell number in each larva was determined. Representative images are shown in D, and quantified results are shown in E. Images are lateral views of the zebrafish yolk sac region with the dorsal side positioned to the top and the anterior to the left. *n*=42–66. Data in A–C and E are presented as mean±s.e.m. ****P<0.0001; ns, not significant (one-way ANOVA followed by Tukey's multiple comparison test in A–C,E).

signal intensity. This is particularly relevant to the data shown in Fig. 2F. Although a significant reduction in ER-LAR-GECO-1 signal was detected, the possibility that other factors such as altered ER-LAR-GECO-1 protein expression may be involved cannot be ruled out. Clearly, more studies are needed to measure Ca^{2+} dynamics with greater precision using a ratiometric ER Ca^{2+} reporter with a greater K_d value. A possible candidate reporter is the calcium-measuring organelle-entrapped protein indicator 1 in the ER (CEPIA1er; Suzuki et al., 2014). CEPIA1er is a variant of GCaMP2 that can emit green, red or blue-green fluorescence. It has a KDEL motif and a Ca^{2+} K_d value of 558 µM (Suzuki et al., 2014). It will be important to generate CEPIA1er reporter fish and perform more *in vivo* imaging experiments to determine the dynamics of $[Ca^{2+}]_{ER}$ changes and the state of luminal ER Ca^{2+} refilling upon the low [Ca^{2+}] stress and BAPTA-AM treatment in the future.

MATERIALS AND METHODS

Ethics statement

All experiments reported were conducted following a protocol approved by the University of Michigan Institutional Committee on the Use and Care of Animals.

Zebrafish husbandry

Zebrafish were raised according to standard zebrafish husbandry guidelines (Westerfield, 2000). Embryos were obtained by natural crosses and raised in standard E3 embryo medium (containing 0.33 mM Ca^{2+}; Westerfield, 2000) unless specified otherwise. Embryos were staged as described previously (Kimmel et al., 1995). In addition to the E3 embryo medium, two additional embryo rearing media containing either 0.001 mM Ca^{2+} (referred to as low [Ca^{2+}] embryo medium) or 0.2 mM Ca^{2+} (referred to as normal [Ca^{2+}] embryo medium) were prepared and used as previously reported (Dai et al., 2014). In some experiments, 0.003% (w/v) N-phenylthiourea (PTU) was added to prevent pigmentation. The generation of *Tg(igfbp5a:GFP)* fish, *Tg(igfbp5a:GCaMP7a)* fish and *trpv6*$^{-/-}$ fish has been reported previously (Liu et al., 2017).

Chemicals and reagents

All reagents were purchased from Sigma-Aldrich (St Louis, MO, USA), unless stated otherwise. BAPTA-AM and W-7 hydrochloride were purchased from Calbiochem (Gibbstown, NJ, USA). Calmidazolium chloride, dantrolene and ryanodine were purchased from Tocris Bioscience (Bristol, UK). STO-609 was purchased from Enzo Life Sciences (Farmingdale, NY, USA). Xestospongin C was purchased from Focus Biomolecules (Plymouth Meeting, PA, USA). The phospho-Akt (S473) and phospho-Akt (T308) rabbit monoclonal antibodies were purchased from Cell Signaling Technology (Danvers, MA, USA). See Table S2 for further details. Restriction enzymes were purchased from New England BioLabs (Ipswich, MA, USA). Primers were purchased from Invitrogen (Carlsbad, CA, USA).

Plasmid construction and BAC constructs

The ER-LAR-GECO-1 cassette was amplified from the CMV-ER-LAR-GECO-1 plasmid (Addgene 61244) and integrated into a kanamycin

Journal of Cell Science (2021) 134, jcs253807. doi:10.1242/jcs.253807

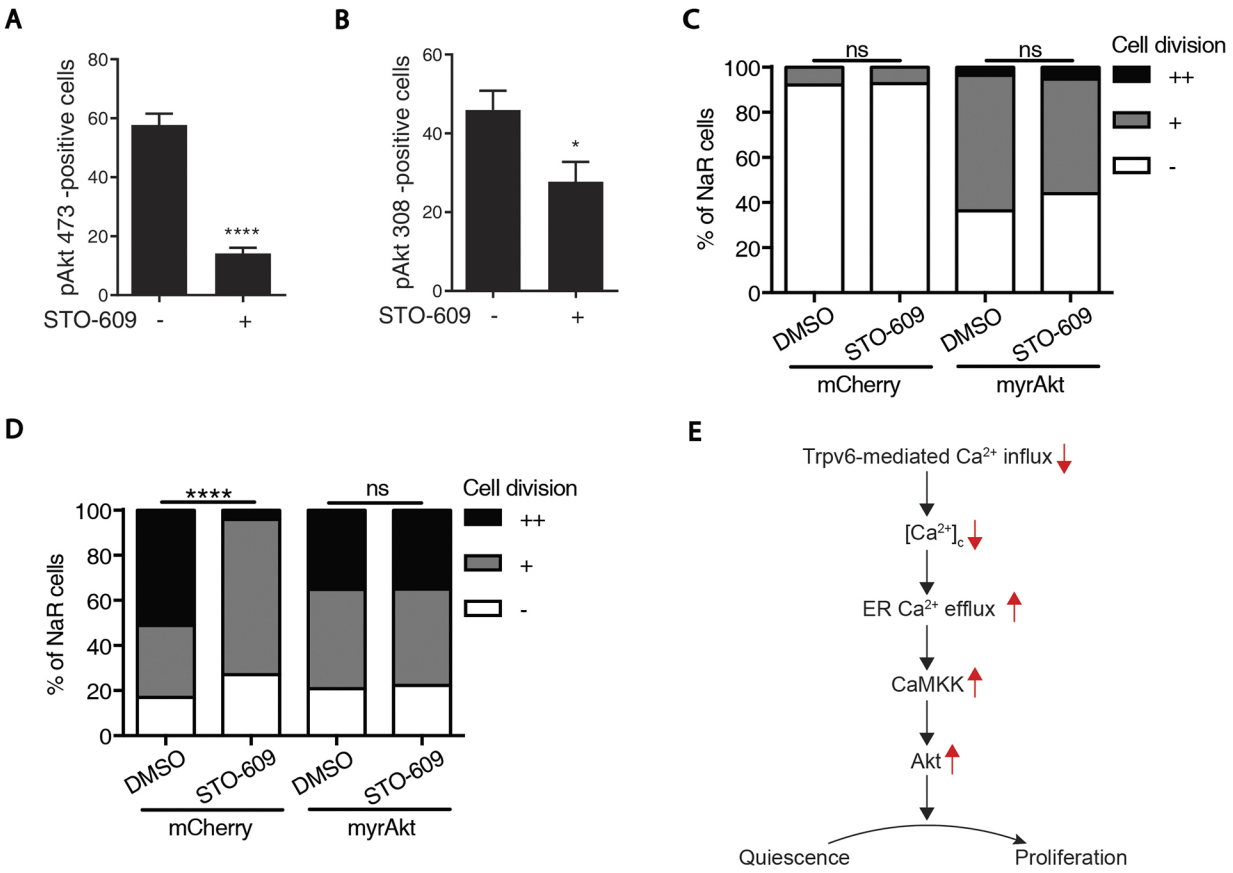

Fig. 6. CaMKK promotes NaR cell reactivation via Akt signaling. (A,B) Effect of STO-609. Wild-type zebrafish were transferred to low [Ca^{2+}] embryo medium containing DMSO or 10 µM STO-609 at 3 dpf. One day later, they were subjected to (A) phospho-Akt (S473) or (B) phospho-Akt (T308) immunostaining. Phospho-Akt-positive cells in the yolk sac region in each larva were quantified. *n*=24–28 (A) and *n*=11–13 (B). Data are presented as mean±s.e.m. (C,D) Effect of myrAkt expression in NaR cells. *Tg(igfbp5a:GFP)* embryos injected with *BAC (igfbp5a:mCherry)* or *BAC (igfbp5a:myr-Akt-mCherry)* were raised. At 3 dpf, they were transferred to normal [Ca^{2+}] embryo medium (C) or low [Ca^{2+}] embryo medium (D) containing DMSO or 10 µM STO-609. At 5 dpf, NaR cells labeled by both GFP and mCherry were scored following a previously established scoring system (Liu et al., 2018). NaR cells that that did not divide, divided once or divided twice are scored as –,+and ++, respectively. *n*=8–29. **P*<0.05; *****P*<0.0001; ns, not significant (two-tailed unpaired t-test in A,B; chi-square test in C,D). (E) Proposed working model of the regulation of cell quiescence-proliferation balance by Ca^{2+}–CaMKK–Akt signaling.

resistance gene-carrying plasmid (Addgene #23007) using the following primers: BglII-ER-F and ER-stop-NotI-R (Table S1). The resulting ER-LAR-GECO-1-Kana cassette was then amplified by PCR and integrated into the *igfbp5aBAC* construct as reported previously (Liu et al., 2017), using primers igfbp5a-ER-LAR-f and igfbp5a-pEGFP-C3-kan-R (Table S1). This resulted in *BAC (igfbp5a:ER-LAR-GECO-1)*. All plasmids were verified by DNA sequencing. The construction of *BAC (igfbp5a:myrAkt-mCherry)* was previously reported (Liu et al., 2018).

Tol2 transposon-mediated genetic mosaic assay

To express transgenes in NaR cells specifically, *BAC (igfbp5a:ER-LAR-GECO-1)* or *BAC (igfbp5a:myrAkt-mCherry)* and Tol2 capped mRNA (synthesized in our laboratory) were mixed and injected into *Tg(igfbp5a:GFP)* or wild-type embryos at the one-cell stage. The embryos were raised and subjected to various treatments. Cells co-expressing mCherry and GFP were identified and imaged as described below or scored for cell division following a previously reported scoring system (Liu et al., 2018).

In vivo Ca^{2+} imaging

The detection of changes in NaR cell $[Ca^{2+}]_c$ was performed using *Tg(igfbp5a:GCaMP7a)* as previously reported (Xin et al., 2019). To detect changes in NaR cell $[Ca^{2+}]_{ER}$, *Tg(igfbp5a:GFP)* embryos were injected with *BAC (igfbp5a:ER-LAR-GECO-1)* at one-cell stage and raised to the 3 d post fertilization (dpf) stage. The larvae were anesthetized, mounted in 1% low-melting point agarose gel and immersed in 1 ml normal [Ca^{2+}] embryo medium. Fish were imaged using a Leica TCS SP8 confocal microscope equipped with an HC PL APO 93×/1.30 GLYC objective. After locating NaR cells using live imaging of the GFP signal (495 nm), ER-LAR-GECO-1 signal was visualized using a filter set of 545/30 nm (excitation) and 620/60 nm (emission). At T_0, a *z*-stack was taken using the xyz-t setting. To start the low [Ca^{2+}] stress treatment, the normal [Ca^{2+}] medium was replaced with the low [Ca^{2+}] medium after three washes. The ER-LAR-GECO-1 signal in the same NaR cell was recorded at 2 h and 18 h. Imaging chambers were covered with microscope cover glass to prevent evaporation. All recorded images were corrected for background fluorescence determined from regions outside NaR cells. $[Ca^{2+}]_{ER}$ values were expressed as F_t/F_0, where F_0 and F_t denote the average fluorescence at the start of the experiment (F_0) and at each time point (F_t), respectively.

Whole-mount immunostaining and *in situ* hybridization

Zebrafish larvae were fixed in 4% paraformaldehyde, permeabilized in methanol and subjected to immunostaining or *in situ* hybridization analysis as reported previously (Dai et al., 2014). Phospho-Akt (Ser473) and Phospho-Akt (Thr308) antibodies (Cell Signaling Technology) were used at 1:200 dilutions.

Transient gene knockout

sgRNAs targeting *camkk1a*, *camkk1b*, *camkk2* and *stim1a* were designed using CHOPCHOP (http://chopchop.cbu.uib.no/), and their sequences are listed in Table S1. A mixture containing 40 pg sgRNA and 400 pg *cas9*

mRNA (for *camkk* sgRNAs) or 10 pg sgRNAs and 100 pg *cas9* mRNA (for *stim1a*) was injected into one-cell-stage embryos as reported previously (Xin and Duan, 2018). A subset of injected embryos was pooled, and DNA was isolated and analyzed by PCR followed by a hetero-duplex assay performed as reported previously (Liu et al., 2018). After confirming the indels, the remaining injected embryos were used for experiments.

Genotyping

Each larva was digested in 100 µl SZL buffer (50 mM KCl, 2.5 mM $MgCl_2$, 10 mM Tris-HCl pH 8.3, 0.45% NP-40, 0.45% Tween-20 and 0.01% gelatine) containing 100 µg/ml proteinase K for 2 h at 60°C followed by 15 min heat treatment (95°C). The lysate was used as template for a heteroduplex motility assay (HRMA) assay as reported previously (Zhu et al., 2014).

Drug treatment

Drugs used in this study were dissolved in DMSO and further diluted in embryo media. A total of 10–15 fish per well were placed in 12-well plate and washed with either normal or low [Ca^{2+}] embryo medium three times before being treated with 2 ml drug-containing medium. Treatment started at 3 dpf. The samples were collected for immunostaining 1 d after treatment or for NaR cell quantification 2 d after treatment.

Statistical analysis

Values are shown as the mean±s.e.m. Statistical significance among experimental groups was determined using two-tailed unpaired *t*-test, one-way ANOVA followed by Tukey's multiple comparison test, or chi-square test. Statistical significance was accepted at $P<0.05$ or greater.

Acknowledgements

We thank the Duan lab members for valuable discussion and technical assistance.

Competing interests

The authors declare no competing or financial interests.

Author contributions

Conceptualization: C.D.; Formal analysis: Y.X., J.G., Y.L.; Investigation: Y.X., J.G., Y.L.; Resources: C.D.; Data curation: Y.X., J.G., Y.L.; Writing - original draft: Y.X., C.D.; Writing - review & editing: Y.X., J.G., Y.L., C.D.; Visualization: Y.X., J.G., Y.L.; Supervision: C.D.; Project administration: C.D.; Funding acquisition: C.D.

Funding

This work was supported by National Science Foundation grants IOS-1557850 and IOS-1755268 to C.D. The funders had no role in study design, data collection and analysis, decision to publish, or preparation of the manuscript.

Peer review history

The peer review history is available online at https://journals.biologists.com/jcs/article-lookup/doi/10.1242/jcs.253807.

References

Allen, J. R., Skeath, J. B. and Johnson, S. L. (2019). GABA-A receptor and mitochondrial TSPO signaling act in parallel to regulate melanocyte stem cell quiescence in larval zebrafish. *Pigment Cell Melanoma Res.* **33**, 416-425. doi:10.1111/pcmr.12836

Bagur, R. and Hajnóczky, G. (2017). Intracellular Ca^{2+} sensing: its role in calcium homeostasis and signaling. *Mol. Cell* **66**, 780-788. doi:10.1016/j.molcel.2017.05.028

Berchtold, M. W. and Villalobo, A. (2014). The many faces of calmodulin in cell proliferation, programmed cell death, autophagy, and cancer. *Biochim. Biophys. Acta (BBA) Mol. Cell Res.* **1843**, 398-435. doi:10.1016/j.bbamcr.2013.10.021

Biteau, B., Hochmuth, C. E. and Jasper, H. (2011). Maintaining tissue homeostasis: dynamic control of somatic stem cell activity. *Cell Stem Cell* **9**, 402-411. doi:10.1016/j.stem.2011.10.004

Carafoli, E. and Krebs, J. (2016). Why calcium? how calcium became the best communicator. *J. Biol. Chem.* **291**, 20849-20857. doi:10.1074/jbc.R116.735894

Chell, J. M. and Brand, A. H. (2010). Nutrition-responsive glia control exit of neural stem cells from quiescence. *Cell* **143**, 1161-1173. doi:10.1016/j.cell.2010.12.007

Chen, B.-C., Wu, W.-T., Ho, F.-M. and Lin, W.-W. (2002). Inhibition of interleukin-1β-induced NF-κB activation by calcium/calmodulin-dependent protein kinase kinase occurs through Akt activation associated with interleukin-1 receptor-associated kinase phosphorylation and uncoupling of MyD88. *J. Biol. Chem.* **277**, 24169-24179. doi:10.1074/jbc.M106014200

Chen, C., Liu, Y., Liu, R., Ikenoue, T., Guan, K.-L., Liu, Y. and Zheng, P. (2008). TSC–mTOR maintains quiescence and function of hematopoietic stem cells by repressing mitochondrial biogenesis and reactive oxygen species. *J. Exp. Med.* **205**, 2397-2408. doi:10.1084/jem.20081297

Chen, C., Liu, Y., Liu, Y. and Zheng, P. (2009). mTOR regulation and therapeutic rejuvenation of aging hematopoietic stem cells. *Sci. Signal.* **2**, ra75. doi:10.1126/scisignal.2000559

Chen, S., Liu, Y., Rong, X., Li, Y., Zhou, J. and Lu, L. (2017). Neuroprotective role of the Pi3 Kinase/akt signaling pathway in zebrafish. *Front. Endocrinol.* **8**, 21. doi:10.3389/fendo.2017.00021

Cheung, T. H. and Rando, T. A. (2013). Molecular regulation of stem cell quiescence. *Nat. Rev. Mol. Cell Biol.* **14**, 329-340. doi:10.1038/nrm3591

Clapham, D. E. (2007). Calcium signaling. *Cell* **131**, 1047-1058. doi:10.1016/j.cell.2007.11.028

Dai, W., Bai, Y., Hebda, L., Zhong, X., Liu, J., Kao, J. and Duan, C. (2014). Calcium deficiency-induced and TRP channel-regulated IGF1R-PI3K-Akt signaling regulates abnormal epithelial cell proliferation. *Cell Death Differ.* **21**, 568-581. doi:10.1038/cdd.2013.177

Fiore, A. P. Z. P., Ribeiro, P. d. F. and Bruni-Cardoso, A. (2018). Sleeping beauty and the microenvironment enchantment: microenvironmental regulation of the proliferation-quiescence decision in normal tissues and in cancer development. *Front. Cell Dev. Biol.* **6**, 59. doi:10.3389/fcell.2018.00059

Gocher, A. M., Azabdaftari, G., Euscher, L. M., Dai, S., Karacosta, L. G., Franke, T. F. and Edelman, A. M. (2017). Akt activation by Ca^{2+}/calmodulin-dependent protein kinase kinase 2 (CaMKK2) in ovarian cancer cells. *J. Biol. Chem.* **292**, 14188-14204. doi:10.1074/jbc.M117.778464

Gonano, L. A. and Jones, P. P. (2017). FK506-binding proteins 12 and 12.6 (FKBPs) as regulators of cardiac ryanodine receptors: insights from new functional and structural knowledge. *Channels* **11**, 415-425. doi:10.1080/19336950.2017.1344799

Guillot, C. and Lecuit, T. (2013). Mechanics of epithelial tissue homeostasis and morphogenesis. *Science* **340**, 1185-1189. doi:10.1126/science.1235249

Horsley, V., Aliprantis, A. O., Polak, L., Glimcher, L. H. and Fuchs, E. (2008). NFATc1 balances quiescence and proliferation of skin stem cells. *Cell* **132**, 299-310. doi:10.1016/j.cell.2007.11.047

Hwang, P.-P. (2009). Ion uptake and acid secretion in zebrafish (Danio rerio). *J. Exp. Biol.* **212**, 1745-1752. doi:10.1242/jeb.026054

Kahl, C. R. and Means, A. R. (2003). Regulation of cell cycle progression by calcium/calmodulin-dependent pathways. *Endocr. Rev.* **24**, 719-736. doi:10.1210/er.2003-0008

Kamei, H., Yoneyama, Y., Hakuno, F., Sawada, R., Shimizu, T., Duan, C. and Takahashi, S.-I. (2018). Catch-up growth in zebrafish embryo requires neural crest cells sustained by Irs1 signaling. *Endocrinology* **159**, 1547-1560. doi:10.1210/en.2017-00847

Karacosta, L. G., Foster, B. A., Azabdaftari, G., Feliciano, D. M. and Edelman, A. M. (2012). A regulatory feedback loop between Ca2+/calmodulin-dependent protein kinase kinase 2 (CaMKK2) and the androgen receptor in prostate cancer progression. *J. Biol. Chem.* **287**, 24832-24843. doi:10.1074/jbc.M112.370783

Kimmel, C. B., Ballard, W. W., Kimmel, S. R., Ullmann, B. and Schilling, T. F. (1995). Stages of embryonic development of the zebrafish. *Dev. Dyn.* **203**, 253-310. doi:10.1002/aja.1002030302

Kohn, A. D., Takeuchi, F. and Roth, R. A. (1996). Akt, a pleckstrin homology domain containing kinase, is activated primarily by phosphorylation. *J. Biol. Chem.* **271**, 21920-21926. doi:10.1074/jbc.271.36.21920

Kovacs, G., Danko, T., Bergeron, M. J., Balazs, B., Suzuki, Y., Zsembery, A. and Hediger, M. A. (2011). Heavy metal cations permeate the TRPV6 epithelial cation channel. *Cell Calcium* **49**, 43-55. doi:10.1016/j.ceca.2010.11.007

Lin, F., Marcelo, K. L., Rajapakshe, K., Coarfa, C., Dean, A., Wilganowski, N., Robinson, H., Sevick, E., Bissig, K.-D., Goldie, L. C. et al. (2015). The camKK2/camKIV relay is an essential regulator of hepatic cancer. *Hepatology* **62**, 505-520. doi:10.1002/hep.27832

Liu, D.-M., Wang, H.-J., Han, B., Meng, X.-Q., Chen, M.-H., Yang, D.-B., Sun, Y., Li, Y.-L. and Jiang, C.-L. (2016). CAMKK2, regulated by promoter methylation, is a prognostic marker in diffuse gliomas. *CNS Neurosci. Ther.* **22**, 518-524. doi:10.1111/cns.12531

Liu, C., Dai, W., Bai, Y., Chi, C., Xin, Y., He, G., Mai, K. and Duan, C. (2017). Development of a whole organism platform for phenotype-based analysis of IGF1R-PI3K-Akt-Tor Action. *Sci. Rep.* **7**, 1994. doi:10.1038/s41598-017-01687-3

Liu, C., Xin, Y., Bai, Y., Lewin, G., He, G., Mai, K. and Duan, C. (2018). Ca^{2+} concentration–dependent premature death of igfbp5a$^{-/-}$ fish reveals a critical role of IGF signaling in adaptive epithelial growth. *Sci. Signal.* **11**, eaat2231. doi:10.1126/scisignal.aat2231

Liu, C., Li, S., Noer, P. R., Kjaer-Sorensen, K., Juhl, A. K., Goldstein, A., Ke, C., Oxvig, C. and Duan, C. (2020). The metalloproteinase Papp-aa controls epithelial cell quiescence-proliferation transition. *eLife* **9**, e52322. doi:10.7554/eLife.52322

Luchsinger, L. L., Strikoudis, A., Danzl, N. M., Bush, E. C., Finlayson, M. O., Satwani, P., Sykes, M., Yazawa, M. and Snoeck, H.-W. (2019). Harnessing

hematopoietic stem cell low intracellular calcium improves their maintenance in vitro. *Cell Stem Cell* **25**, 225-240.e7. doi:10.1016/j.stem.2019.05.002

Ma, Z., Wen, D., Wang, X., Yang, L., Liu, T., Liu, J., Zhu, J. and Fang, X. (2016). Growth inhibition of human gastric adenocarcinoma cells in vitro by STO-609 is independent of calcium/calmodulin-dependent protein kinase kinase-beta and adenosine monophosphate-activated protein kinase. *Am. J. Transl. Res.* **8**, 1164-1171.

MacMillan, D. (2013). FK506 binding proteins: cellular regulators of intracellular Ca2+ signalling. *Eur. J. Pharmacol.* **700**, 181-193. doi:10.1016/j.ejphar.2012.12.029

Olianas, M. C., Dedoni, S. and Onali, P. (2018). Muscarinic acetylcholine receptors potentiate 5′-adenosine monophosphate-activated protein kinase stimulation and glucose uptake triggered by thapsigargin-induced store-operated Ca^{2+} entry in human neuroblastoma cells. *Neurochem. Res.* **43**, 245-258. doi:10.1007/s11064-017-2410-x

Pan, T.-C., Liao, B.-K., Huang, C.-J., Lin, L.-Y. and Hwang, P.-P. (2005). Epithelial Ca^{2+} channel expression and Ca^{2+} uptake in developing zebrafish. *Am. J. Physiol. Regul. Integr. Comp. Physiol.* **289**, R1202-R1211. doi:10.1152/ajpregu.00816.2004

Prakriya, M. and Lewis, R. S. (2015). Store-operated calcium channels. *Physiol. Rev.* **95**, 1383-1436. doi:10.1152/physrev.00020.2014

Schmitt, J. M., Smith, S., Hart, B. and Fletcher, L. (2012). CaM kinase control of AKT and LNCaP cell survival. *J. Cell Biochem.* **113**, 1514-1526. doi:10.1002/jcb.24020

Shima, T., Mizokami, A., Miyagi, T., Kawai, K., Izumi, K., Kumaki, M., Ofude, M., Zhang, J., Keller, E. T. and Namiki, M. (2012). Down-regulation of calcium/calmodulin-dependent protein kinase kinase 2 by androgen deprivation induces castration-resistant prostate cancer. *Prostate* **72**, 1789-1801. doi:10.1002/pros.22533

Subbannayya, Y., Syed, N., Barbhuiya, M. A., Raja, R., Marimuthu, A., Sahasrabuddhe, N., Pinto, S. M., Manda, S. S., Renuse, S., Manju, H. C. et al. (2015). Calcium calmodulin dependent kinase kinase 2 - a novel therapeutic target for gastric adenocarcinoma. *Cancer Biol. Ther.* **16**, 336-345. doi:10.4161/15384047.2014.972264

Suzuki, J., Kanemaru, K., Ishii, K., Ohkura, M., Okubo, Y. and Iino, M. (2014). Imaging intraorganellar Ca^{2+} at subcellular resolution using CEPIA. *Nat. Commun.* **5**, 4153. doi:10.1038/ncomms5153

Swulius, M. T. and Waxham, M. N. (2008). Ca^{2+}/calmodulin-dependent protein kinases. *Cell. Mol. Life Sci.* **65**, 2637-2657. doi:10.1007/s00018-008-8086-2

Tai, K., Cockburn, K. and Greco, V. (2019). Flexibility sustains epithelial tissue homeostasis. *Curr. Opin. Cell Biol.* **60**, 84-91. doi:10.1016/j.ceb.2019.04.009

Tokumitsu, H. and Soderling, T. R. (1996). Requirements for calcium and calmodulin in the calmodulin kinase activation cascade. *J. Biol. Chem.* **271**, 5617-5622. doi:10.1074/jbc.271.10.5617

Umemoto, T., Hashimoto, M., Matsumura, T., Nakamura-Ishizu, A. and Suda, T. (2018). Ca^{2+}–mitochondria axis drives cell division in hematopoietic stem cells. *J. Exp. Med.* **215**, 2097-2113. doi:10.1084/jem.20180421

Voets, T., Janssens, A., Droogmans, G. and Nilius, B. (2004). Outer pore architecture of a Ca2+-selective TRP channel. *J. Biol. Chem.* **279**, 15223-15230. doi:10.1074/jbc.M312076200

Wang, N., Yao, M., Xu, J., Quan, Y., Zhang, K., Yang, R. and Gao, W.-Q. (2015). Autocrine Activation of CHRM3 promotes prostate cancer growth and castration resistance via CaM/CaMKK-mediated phosphorylation of Akt. *Clin. Cancer Res.* **21**, 4676-4685. doi:10.1158/1078-0432.CCR-14-3163

Westerfield, M. (2000). *The Zebrafish Book. A Guide for the Laboratory Use of Zebrafish (Danio rerio)*. 4th edn. Eugene: University of Oregon Press. http://zfin.org/zf_info/zfbook/zfbk.html

Wu, J., Prole, D. L., Shen, Y., Lin, Z., Gnanasekaran, A., Liu, Y., Chen, L., Zhou, H., Chen, S. R. W., Usachev, Y. M. et al. (2014). Red fluorescent genetically encoded Ca2+ indicators for use in mitochondria and endoplasmic reticulum. *Biochem. J.* **464**, 13-22. doi:10.1042/BJ20140931

Xin, Y. and Duan, C. (2018). Microinjection of antisense morpholinos, CRISPR/Cas9 RNP, and RNA/DNA into zebrafish embryos. In *Hypoxia* (ed. L. E. Huang), pp. 205-211. New York, NY: Humana Press. doi:10.1007/978-1-4939-7665-2_18

Xin, Y., Malick, A., Hu, M., Liu, C., Batah, H., Xu, H. and Duan, C. (2019). Cell-autonomous regulation of epithelial cell quiescence by calcium channel Trpv6. *eLife* **8**, e48003. doi:10.7554/eLife.48003

Yan, J.-J. and Hwang, P.-P. (2019). Novel discoveries in acid-base regulation and osmoregulation: a review of selected hormonal actions in zebrafish and medaka. *Gen. Comp. Endocrinol.* **277**, 20-29. doi:10.1016/j.ygcen.2019.03.007

Yang, Z., Yan, H., Dai, W., Jing, J., Yang, Y., Mahajan, S., Zhou, Y., Li, W., Macaubas, C., Mellins, E. D. et al. (2019). Tmem178 negatively regulates store-operated calcium entry in myeloid cells via association with STIM1. *J. Autoimmun.* **101**, 94-108. doi:10.1016/j.jaut.2019.04.015

Yano, S., Tokumitsu, H. and Soderling, T. R. (1998). Calcium promotes cell survival through CaM-K kinase activation of the protein-kinase-B pathway. *Nature* **396**, 584-587. doi:10.1038/25147

Zhu, X., Xu, Y., Yu, S., Lu, L., Ding, M., Cheng, J., Song, G., Gao, X., Yao, L., Fan, D. et al. (2014). An efficient genotyping method for genome-modified animals and human cells generated with CRISPR/Cas9 system. *Sci. Rep.* **4**, 6420. doi:10.1038/srep06420

Ziegler, A. N., Levison, S. W. and Wood, T. L. (2015). Insulin and IGF receptor signalling in neural-stem-cell homeostasis. *Nat. Rev. Endocrinol.* **11**, 161-170. doi:10.1038/nrendo.2014.208

Ziegler, A. N., Feng, Q., Chidambaram, S., Testai, J. M., Kumari, E., Rothbard, D. E., Constancia, M., Sandovici, I., Cominski, T., Pang, K. et al. (2019). Insulin-like growth factor II: an essential adult stem cell niche constituent in brain and intestine. *Stem Cell Rep.* **12**, 816-830. doi:10.1016/j.stemcr.2019.02.011

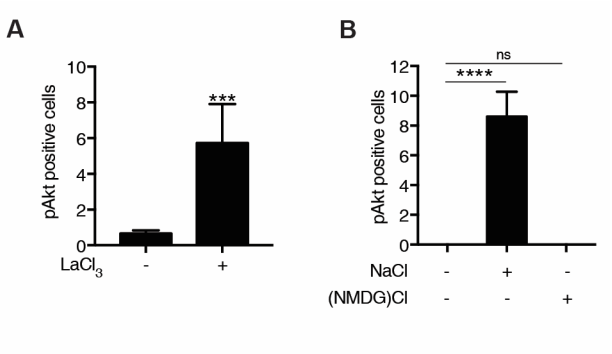

Fig. S1. (A-B) Wild-type larvae were treated with 100 µM $LaCl_3$, 100 mM NaCl or 100 mM (NMDG)Cl from 3 dpf to 4 dpf. They were fixed and analyzed by phospho-Akt (S473) immunostaining. pAkt-positive cells were quantified. Data are shown as mean ± SEM. n = 11~32 (A) or 15~16 (B), ***$P < 0.001$ by unpaired t-test (A). **** indicates $P < 0.0001$ by one-way ANOVA followed by Tukey's multiple comparison test (B).

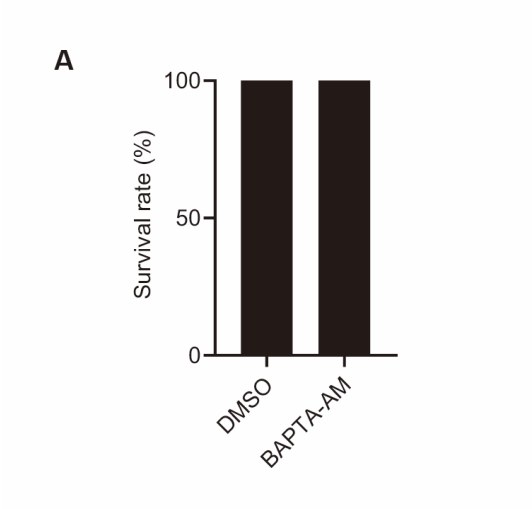

Fig. S2. Effect of BAPTA-AM on embryo viability. Wild-type embryos were treated with 100 µM BAPTA-AM from 3 dpf to 5 dpf. Viable larvae were quantified. Data are show as % of viable larvae. n=12.

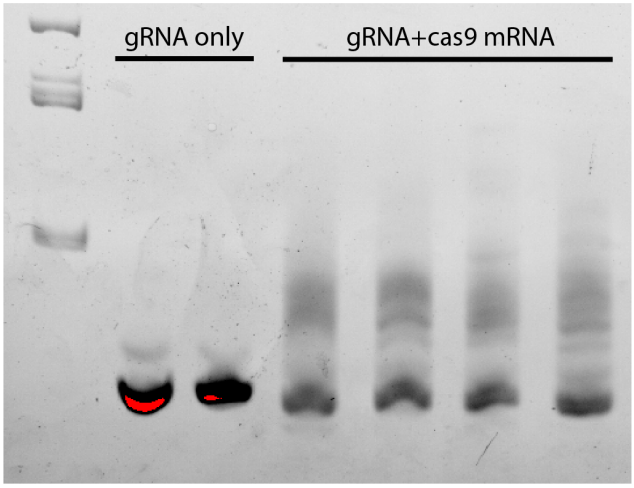

Fig. S3. Transient knockdown of *stim1a*. Embryos injected with a mixture of *stim1a* gRNAs and *cas9* mRNA or gRNAs alone were raised in E3 embryo medium to 1 dpf. Each embryo was lysed individually and analyzed by PCR followed by hetero-duplex motility assay.

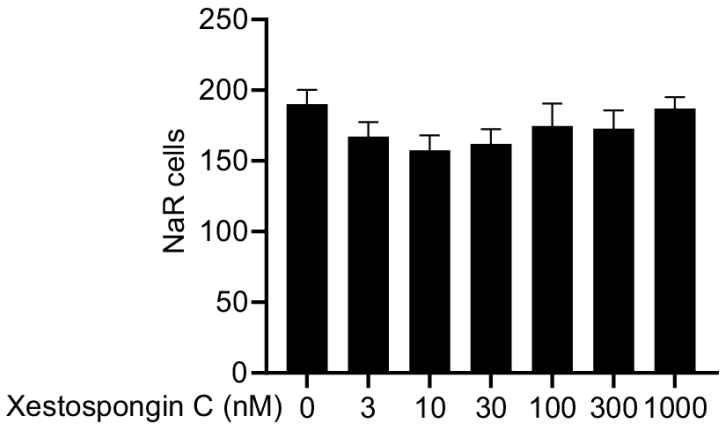

Fig. S4. Effect of IP3 receptor inhibition. *Tg(igfbp5a:GFP)* larvae were treated with DMSO or Xestospongin C at the indicated concentrations in the low [Ca^{2+}] embryo medium from 3 dpf to 5 dpf. NaR cell in each larva was quantified at 5 dpf. Data are shown as mean ± SEM. n= 9-10. No statistical difference was detected among these groups.

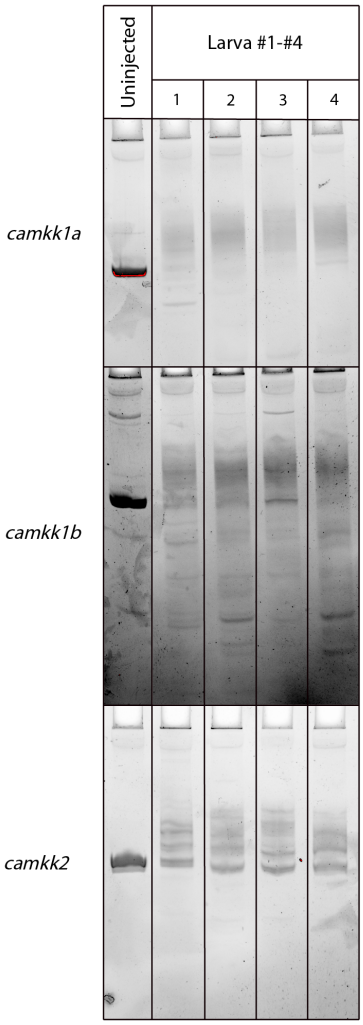

Fig. S5. Transient knockdown of *camkk* genes. Embryos injected with gRNAs and *cas9* mRNA were raised in standard E3 embryo medium to 1 dpf. Each embryo was lysed individually and analyzed by PCR followed by hetero-duplex motility assay. Representative images of un-injected and injected embryos are shown.

Table S1. Primer and gRNA sequences

Name	Sequences
BglII-ER-F	5'-gaagatctATGCTGCTGCCCGTCCCCCT-3'
ER-stop-NotI-R	5'-atttgcggccgcTTACAGCTCGTCCTTCTTCG-3'
igfbp5a-ER-LAR-f	5'-GTTTTGCCATTTCAAAGCTGGTGAAATAGGTGTTCTACAGTAGGACGATGCTGCTGCCCGTCCCCCT -3'
igfbp5a-pEGFP-C3-kan-R	5'-GTTTACTTTTGTCCCATATAAAACAAATACTACAAGTCAATAAAACATACAGAACTCCAGCATGAGATCCCCGC-3'
camkk1a-sgRNA1	5'-GGACACTCGTTTGGATTCGA-3'
camkk1a-sgRNA2	5'-GCCAGACAGGTGTGGCCTCT-3'
camkk1b-sgRNA1	5'-GGTCCTGTACCCGTTTGGTG-3'
camkk1b-sgRNA2	5'-GCAGCTGGATCTCTCCTGCA-3'
camkk2-sgRNA1	5'-GTTTGTAGAGCCGTGATGG-3'
camkk2-sgRNA2	5'-GCAGGTCCTGGAAGTAGAAG-3'

Table S2. Fish lines and Reagents

Reagent type (species) or resource	Designation	Source or reference	Identifiers
strain, strain background (*Danio rerio*)	*Tg(igfbp5a:GCaMP7a)*	Pubmed ID: 31526479	
strain, strain background (*Danio rerio*)	*Tg(igfbp5a:GFP)*	Pubmed ID: 28515443	
strain, strain background (*Danio rerio*)	*trpv6 Δ7; Tg(igfbp5a:GFP)*	Pubmed ID: 31526479	
chemical compound, drug	Lanthanum(III) chloride	Sigma-Aldrich	Catalog no.: 449830-5G
chemical compound, drug	Thapsigargin	Sigma-Aldrich	Catalog no.: T9033
chemical compound, drug	Cyclopiazonic acid	Sigma-Aldrich	Catalog no.: C1530
chemical compound, drug	BAPTA-AM	Sigma-Aldrich	Catalog no.: A1076
chemical compound, drug	STO-609	Enzo Life Sciences	Catalog no.: BML-EI389
chemical compound, drug	W-7	Calbiochem	Catalog no.: 681629
chemical compound, drug	Calmidazolium chloride	Tocris Bioscience	Catalog no.: 2561
chemical compound, drug	Ryanodine	Tocris Bioscience	Catalog no.: 1329
chemical compound, drug	Dantrolene	Tocris Bioscience	Catalog no.: 0507
chemical compound, drug	Xestospongin C	Focus Biomolecules	Catalog no.: 10-1207
Antibody	Phospho-Akt (Ser473)	Cell Signaling Technology	Catalog no.: 4060
Antibody	Phospho-Akt (Ser)	Cell Signaling Technology	Catalog no.: 4056
Genetic reagent	ER-LAR-GECO1	Addgene	Catalog no.: 61244
Genetic reagent	*BAC (igfbp5a:myrAkt-IRES2-mCherry)*	Pubmed ID: 28515443	